Development of theoretical oxygen saturation calibration curve based on optical density ratio and optical simulation approach

Cite as: AIP Conference Proceedings **1883**, 020024 (2017); https://doi.org/10.1063/1.5002042
Published Online: 14 September 2017

Nur Anida Jumadi, Gan Kok Beng, Mohd Alauddin Mohd Ali, Edmond Zahedi, Marlia Morsin, et al.

Development of Theoretical Oxygen Saturation Calibration Curve Based on Optical Density Ratio and Optical Simulation Approach

Nur Anida Jumadi [1, a)], Gan Kok Beng [2, 3, b)], Mohd Alauddin Mohd Ali [2, 3], Edmond Zahedi [2] and Marlia Morsin [1,4, c)]

[1] *Department of Electronics Engineering, Universiti Tun Hussein Onn Malaysia, 86400 Parit Raja, Johor , Malaysia*
[2.] *Institute of Space Science, Universiti Kebangsaan Malaysia, 43600 Bangi, Selangor, Malaysia*
[3.] *Department of Electrical, Electronic and Systems Engineering, Universiti Kebangsaan Malaysia, 43600 Bangi, Selangor, Malaysia*
[4]*Institute of Microelectronics & Nanotechnology - Shamsuddin Research Centre (MiNT-SRC), Universiti Tun Hussein Onn Malaysia, 86400 Parit Raja, Johor, Malaysia*

[a)]Corresponding author: anida@uthm.edu.my
[b)]kok_beng_gan@yahoo.com
[c)]marlia@uthm.edu.my

Abstract. The implementation of surface-based Monte Carlo simulation technique for oxygen saturation (S_aO_2) calibration curve estimation is demonstrated in this paper. Generally, the calibration curve is estimated either from the empirical study using animals as the subject of experiment or is derived from mathematical equations. However, the determination of calibration curve using animal is time consuming and requires expertise to conduct the experiment. Alternatively, an optical simulation technique has been used widely in the biomedical optics field due to its capability to exhibit the real tissue behavior. The mathematical relationship between optical density (OD) and optical density ratios (ODR) associated with S_aO_2 during systole and diastole is used as the basis of obtaining the theoretical calibration curve. The optical properties correspond to systolic and diastolic behaviors were applied to the tissue model to mimic the optical properties of the tissues. Based on the absorbed ray flux at detectors, the OD and ODR were successfully calculated. The simulation results of optical density ratio occurred at every 20 % interval of S_aO_2 is presented with maximum error of 2.17 % when comparing it with previous numerical simulation technique (MC model). The findings reveal the potential of the proposed method to be used for extended calibration curve study using other wavelength pair.

INTRODUCTION

Oxygen saturation, S_aO_2 can be measured using pulse oximeter. The pulse oximeter is developed based on the light absorption by the oxyhemoglobin (HbO_2) and deoxyhemoglobin (Hb). The reflected or transmitted optical signal from the tissue are detected by the photo detector and known as photoplethysmogram (PPG). The optode can be formed by using a pair of light source and detector to the array of optical sensors. The S_aO_2 value is obtained by finding the ratio of ac signal over dc signal of red and infrared light source. This ratio is then mapped with the corresponding S_aO_2 based on the calibration curve. Fig. 1 shows an example of the empirical calibration curve of pulse oximeter for 660/890nm wavelength pair. This wavelength pair is widely used in standard pulse oximeter.

Usually, the calibration curve will be done empirically by controlling and reducing the S_aO_2 level in the animal. The S_aO_2 level will match with the AC/DC ratio of the wavelength pair. However, conducting empirical experiment on the animal requires expertise and time consuming. A specific procedures such as minor surgery on the animal are required in order to control the oxygen level in it's body [1]. On different note, the empirical calibration experiment can also be done on human. However, to establish the calibration curve for oxygen level below 35% are hazardous

Advances in Electrical and Electronic Engineering: From Theory to Applications
AIP Conf. Proc. 1883, 020024-1–020024-10; doi: 10.1063/1.5002042
Published by AIP Publishing. 978-0-7354-1563-8/$30.00

to human being since reducing the oxygen level up to that point could damage to the brain function. Previous literatures showed that numerical simulation approach such as Monte Carlo (MC) algorithm and Photon Diffusion (PD) equation can be used to establish the calibration curve for 660nm and 890nm wavelength pair [2-3]. The calibration curve was successfully developed using those methods but an extensive readings and understanding on the algorithm as well as equations may hinder interested researcher whom lack of fundamental knowledge from exploring the concept of calibration curve in pulse oximeter.

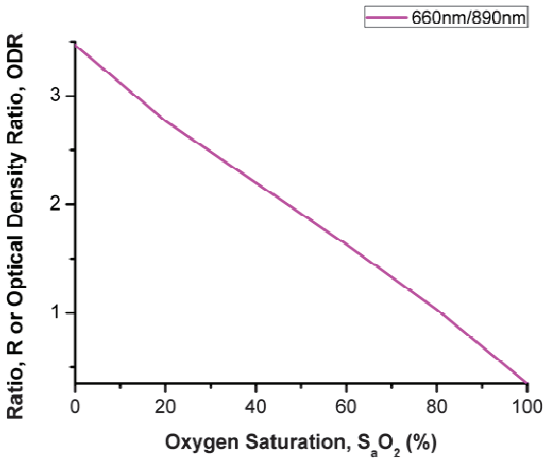

FIGURE 1. An example of empirical calibration curve [4]

Therefore, this paper will address the development of the theoretical calibration curve using commercial optical simulation software namely as Advanced Simulation Analysis Program (ASAP) to counter the limitations mentioned above. Besides easy-written code, this software is able to simulate the optical characteristics of the living tissue specimen and produce the desired output that mimics to the tissue behavior. Moreover, the propagation of lights in the tissue is modeled based on the nature of light when interacting within the tissue. In other words, it is able to experience multiple scattering as well as being absorbed by the defined tissue structures. In addition, not only the tissue can be modeled in three dimensions, even the propagation of the lights can be visualized during the ray tracing procedure.

In order to achieve the objective, the 660 nm and 890 nm wavelength pair was used as a pilot study. The determination of AC over DC ratio of two different wavelengths was based on the relationship between optical density ratio and S_aO_2. In this paper, the relationship of optical density ratio using optical properties at systolic and diastolic (SD) states will be defined mathematically. Explanation and discussion about the physiological conditions during SD with the Photoplethysmography (PPG) signal in the mathematical view was given to help the readers to understand the derivation of optical density ratio.

The development of theoretical calibration curve in this case study was dependent on the optical properties definition. Therefore, the optical properties during systole and diastole for other S_aO_2 values were clearly defined and presented in this paper based on the established literatures. The results obtained in this study were compared with the previous reported data for validation purpose. The scope of this project is limited to: i. Employ optical properties associate with SD conditions at 20, 40, 60, 80 and 100 % of S_aO_2 at 660 nm and 890 nm; ii. The arrangement of emitter and detector (sensor) was in reflectance mode and iii. The resulted optical density ratio is based on the sensor spacing of 12 mm.

BACKGROUND STUDY

Photoplethysmograph and Absorption Spectra

The waveform shown in Fig. 2 is a recorded PPG signal at infrared band. This PPG waveform is useful in providing the heart rate and S_aO_2 readings of arterial blood. The PPG signal is generally characterized by two

attributes namely as DC and AC PPG. The pulsatile waveform or also known as AC PPG is resulted from the light absorption by the pulsating arterial blood. On the other hand, the residual arterial blood, venous blood, bloodless tissue, bones and etc. contribute the DC PPG component. The S_aO_2 can be calculated from the PPG waveform due to the difference in the absorption spectra of two different wavelengths.

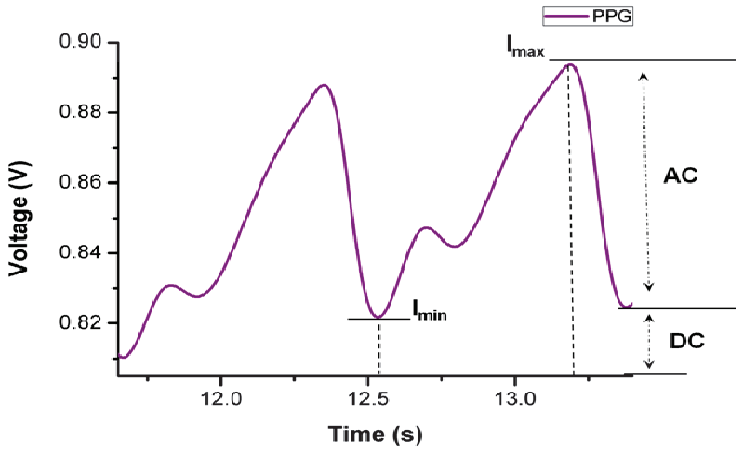

FIGURE 2. The component of light attenuation in the PPG waveform. The I_{max} and I_{min} are the light intensity during diastole and systole, respectively

On the other hand, Fig. 3 shows the difference in the absorptions spectra of oxygenated and reduced hemoglobin from 600 nm to 1000 nm. The 805nm wavelength known as isobestic wavelength; is the point where the absorption spectra of oxygenated and reduced hemoglobin absorbs an equal amount of light. It can be seen clearly that for any wavelength that is below 805 nm, for instance; 660 nm, the reduced hemoglobin of the blood absorbs more red light than the oxygenated hemoglobin whereas for wavelength above 805 nm, the oxygenated hemoglobin absorbs more infrared light than the reduced hemoglobin. Therefore, if 660 nm LED is operated, the reduced hemoglobin is dominant at the DC component causing increasing in the DC component magnitude whilst the AC component magnitude will slightly decrease because less oxygenated hemoglobin has been absorbed by the red light. The contrary effect can be seen if 890 nm LED is employed. The magnitude of DC component will be decreased since the reduced hemoglobin is absorbed less by the infrared light since its absorption spectra is more responsive to oxygenated hemoglobin.

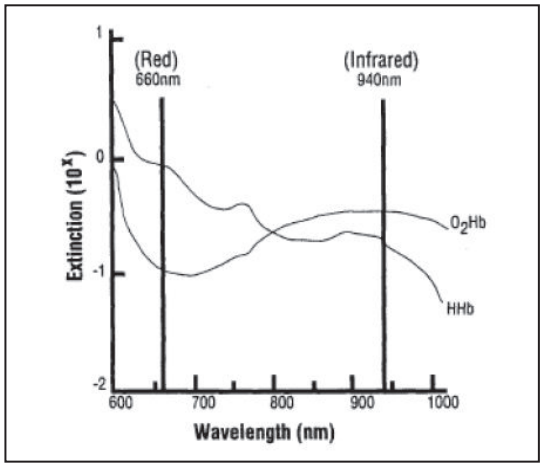

FIGURE 3. Absorption of light from reduced and oxygenated hemoglobin [5]

Light Intensity during Systole & Diastole

Despite direct relationship with the blood pressure, the SD terms are also correlated with human S_aO_2 and their relationship is illustrated in Fig. 2. For example, a normal blood pressure reading, which measured using sphygmomanometer, should be below 120/80 mmHg. The top number, which is known as systolic blood pressure, shows the pressure in the arteries due to the blood being pumped into the arteries during the contraction of the heart. Meanwhile, the bottom number or also calls, as diastolic pressure is the pressure in the arteries when the heart is relaxed after the contraction. As shown in Fig. 2, I_{max} and I_{min} are the maximum and minimum light intensities which occur during diastole and systole; respectively.

To define the light intensity during SD, the optical density, OD of light intensities must be reviewed first. According to the Beer-Lambert law, the light, I_o will be attenuated, I after passing through a sample of medium. Using this information, the OD can be written in the mathematical form as below:

$$OD = \log(I_o / I) \tag{1}$$

Therefore, to incorporate the minimum and maximum intensities of light during SD, (1) can be written as:

$$OD_{sys} = \log(I_o / I_{sys}) \tag{2}$$

$$OD_{dias} = \log(I_o / I_{dias}) \tag{3}$$

Referring again to Fig. 2, during diastole; the light intensity at the tissue, I_{max} is maximal due to the minimum diameter of the arterial vessel plus the absence or reduced of the red blood cell. The light absorbs during diastole will form the DC component of the PPG waveform. Meanwhile, minimum light intensity, I_{min} occurs at systole due to the increasing diameter of the arterial vessel caused by increasing pressure in the arteries and it is also driven by the existence of red blood cell that absorbs the light effectively. Hence, the light absorbs during systole will contribute to the AC pulsatile component of the PPG. The decrease in light intensity which is represented by the difference between I_{dias} and I_{sys}, ΔOD will lead to the resulted ac over dc ratio. Thus; the ratio of ac and dc can be defined as:

$$R_{ac/dc} = \Delta OD = OD_{dias} - OD_{sys} \tag{4}$$

Substitute (2) and (3) into (4), the ac over dc ratio can be written as:

$$R_{ac/dc} = [\log(I_o / I_{dias}) - \log(I_o / I_{sys})] \tag{5}$$

Cancelling the I_o, the ac over dc ratio can be simply estimated as below:

$$R_{ac/dc} = \log(I_{sys} / I_{dias}) \tag{6}$$

The mathematical equation as proved in (6) is also used by [4] in his perturbation analysis for low S_aO_2 using numerical simulation approach. In order to correlate the OD with S_aO_2, an optical density ratio (ODR) at two different wavelengths can be calculated as below:

$$ODR = R_{ac/dc\,\lambda 1} / R_{ac/dc\,\lambda 2} \tag{7}$$

where λ_1 and λ_2 are 660nm and 890nm; respectively.

METHODOLOGY

Optical Properties at Systole and Diastole States

To make any optical simulation becomes meaningful, relevant optical properties for each tissue layer for example; total absorption coefficient (u_a), reduced scattering (u'_s) as well as scattering anisotropy factor, g must be well-defined. Briefly, the total absorption coefficient, $\sum\mu_a$ is calculated as a sum of contributions from the arterial, venous blood and bloodless tissue [4] whereas the reduced scattering coefficients, μ_s' which represents the arbitrary photon diffusions after multiple scattering can be calculated as $u_s(1\text{-}g)$. Meanwhile, to indicate that the photon in the

biological tissue has a high probability of forward scattering, g is assumed to be between 0 and 1. A more detailed explanation on these properties can be referred elsewhere [6].

Figure 4(a) and (b) show the optical properties (absorption coefficient) corresponding to SD at 20, 40, 60, 80 and 100 % of S_aO_2 level visualized in the form of graph for 660 nm and 890 nm; respectively. The total absorption during systole and diastole are calculated based on the oxygenated and reduced hemoglobin translated by [4] from data presented in [7]. To obtain the optical properties at systole, the blood volume in the arterial is assumed to increase by 5 % [4].

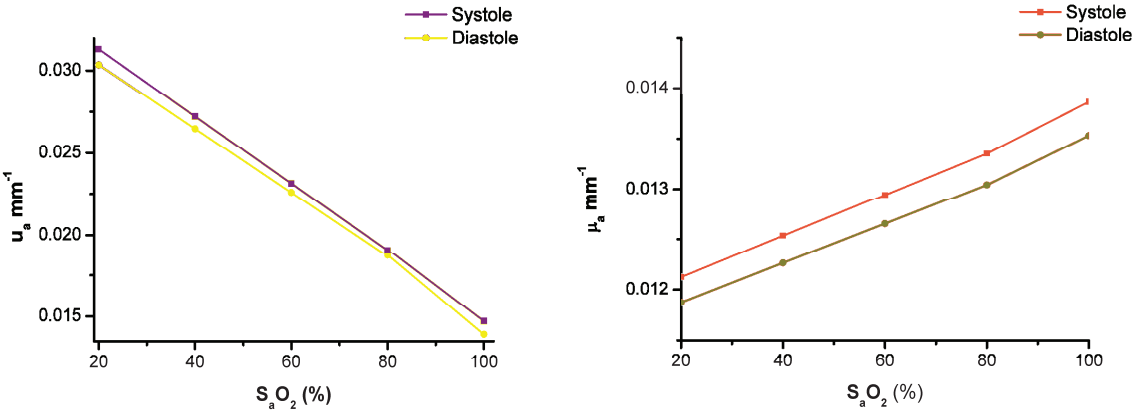

(a) (b)

FIGURE 4. Absorption coefficient, u_a for: (a) 660nm and (b) 890nm

TABLE 1. Other optical characteristics defined during simulation

Optical Properties Characteristics	660nm	890nm
Reduced scattering coefficient, u's (mm^{-1})	1.43	0.89
Anisotropy factor, g	0.8	
Tissue refractive index, n	1.4	

Optical Simulation: Method & Algorithm

There are four main steps required before the ray of photons can be launched into the optical system and these steps will be discussed briefly. First of all, a cylindrical single layer tissue model is developed with a thickness of 10 mm as to mimic the tissue of the finger. In this step, the optical properties at systolic or diastolic will be embedded into the tissue. Since the sensor is arranged in the reflectance mode, the detector must be placed adjacent to the emitter (on the top surface of the tissue); reflecting the common situation when applying reflectance sensor of pulse oximeter. The emitter to detector spacing is measured 12 mm center to center [4]. The detector must be defined as a perfect absorber so that any light that successfully hits the detector can be recorded. Next step is to simulate the emitter, which is located at the origin (0, 0, 0). Here, the emitter is assumed as an incoherent light source or in other words, it replicates the beam behavior of the light emitting diode (LED).

The ray flux of the LED can be simulated according to the LED's graphical light intensity distribution which can be obtained by using the 'apodized ray flux' method; a technique which is included in this program for manipulating the ray flux of the light. A ray-tracing is the next step to follow with one million of rays is infused into the tissue model with the accumulated flux of 0.1 W. The photon of lights is instructed to radiate through the z-direction or in other words, towards the tissue; mimicking the light behavior. Finally, an analysis is carried out by issuing the STATS command. The STAT command will output statistical ray information such as absorbance flux (measured in Watt) or total number of rays at currently targeted object. The resulted outcome from STAT command will be used for further analysis.

The ASAP algorithms for all four steps mentioned above are described as in Fig. 5 below. Briefly, STEP 1 represents the construction of geometrical tissue structure as well as detector, STEP 2 shows how the light pattern is created based on the graphical ray distribution of the LED, STEP 3 performs the ray tracing process and finally, STEP 4 issuing the command for summary ray analysis.

```
STEP 1: Geometrical Tissue Structure and Detector
!!GEOMETRY
!!TISSUE 1
SURFACE
  PLANE Z 0 ELLIPSE 2@300
  OBJECT 'TISSUE.FRONT'
  INTERFACE COATING BARE AIR M
  ENT OBJECT
PLANE Z 10 ELLIPSE 2@300 'TISSUE.BACK'
  INTERFACE COATING BARE M AIR
  REDEFINE COLOR 5
SURFACE
  TUBE Z 0 300 300, 10 300 300, 0 0
  OBJECT 'TISSUE.SIDE'
  INTERFACE COATING BARE AIR M
  REDEFINE COLOR 5

STEP 2: Creating Light Source (Apodizing Ray Flux)
NRAYS=1000000
BEAMS INCOHERENT GEOMETRIC
WAVELENGTH 890 NM
USERAPOD DIRECTION 1 1
1.0022          SIN[0]
0.9978          SIN[0.5678]
0.9648          SIN[1.388]
0.6079          SIN[3.47]
0.4493          SIN[4.4795]
0.3370          SIN[5.4259]
0.2247          SIN[6.7508]
0.1630          SIN[7.6341]
0.1035          SIN[8.8959]
0.0639          SIN[10.1577]
0.0419          SIN[11.3565]
0.0308          SIN[12.6183]
0.0242          SIN[14.0694]
0.0198          SIN[15.7098]
0.0176          SIN[16.9716]
0.0154          SIN[18.0442]
0.0154          SIN[19.2429]
0.0132          SIN[20.0631]

STEP 3: Ray Tracing
WINDOW Y Z
PLOT FACETS 5 5 0 OVERLAY
TRACE PLOT 100000

STEP 4: Analysis
CONSIDER ONLY DET.1
STATS
RETURN
```

FIGURE 5. ASAP coding to simulate light behaviour in single layer tissue

RESULTS & DISCUSSION

Optical Simulation

Figure 6 represents the outcome of the geometrical tissue structure created using ASAP algorithm (STEP 1). This single tissue layer (labeled A) is treated as a homogenous tissue. Meanwhile, a detector (labeled B) assigned as perfect absorber is placed on the top surface of the tissue layer. Meanwhile, Fig. 7 shows the resulted graphical ray distribution that has been successfully created using coding in STEP 2. The lights penetrate through the tissue is following this pattern. This LED emission pattern is applied for 660 nm and 890 nm wavelengths pair. The half angle of the LED is approximately 10 degrees and the optical power for this LED is set at 0.1 W, which is within acceptable and safety power to be applied on the fetus. The resulted trajectory of ray that penetrates through the tissue can be seen in the inset picture of Fig. 5. Note that the trajectory of the light follows multiple scattering phenomena in the turbid media.

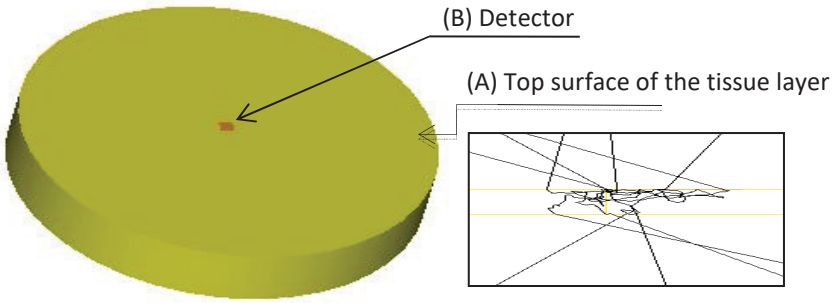

FIGURE 6. Visualization of the tissue structure in ASAP. The inset picture shows the ray tracing of the light.

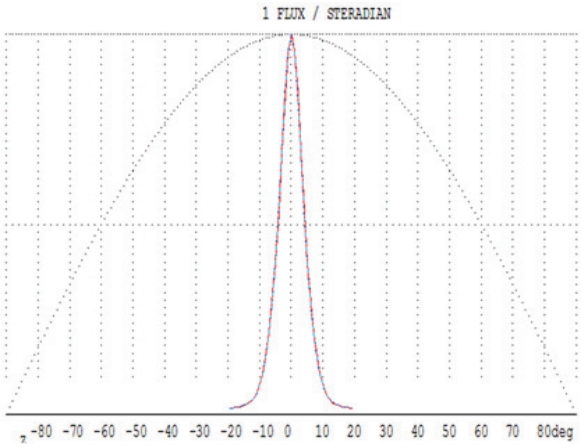

FIGURE 7. The graphical ray distribution created in the software according to Step 2.

Analysis on Absorbed Flux during Systole and Diastole States

In total, there are 20 sets of simulations that have been carried out with an average of 8 minutes for each simulation. Of the 20 simulations, 10 simulations are dedicated for systolic condition while the remaining is for diastolic state. The corresponding parameters (optical tissue coefficients) are calculated according to the real tissue characteristics. This is to ensure that it is able to simulate the tissue behavior as close as possible. The resulted light intensities (measured in milliWatt) accumulated at the detector are presented in Table 2. The light intensity during systole, I_{sys} and light intensity during diastole, I_{dias} is recorded for each level of oxygen saturation. The ratio, R of each wavelength associated with the oxygen level is then obtained by using equation 6.

TABLE 2. The simulated light intensity values during systole and diastole for 660 nm and 890 nm

S_aO_2	660 nm			890 nm		
	I_{sys} (mW)	I_{dias} (mW)	R_{660nm}	I_{sys} (mW)	I_{dias} (mW)	R_{890nm}
20	6.35	6.46	-0.00755	7.22	7.27	-0.00300
40	6.91	7.01	-0.00612	7.14	7.19	-0.00321
60	7.56	7.64	-0.00454	7.06	7.12	-0.00341
80	8.32	8.37	-0.00279	6.99	7.05	-0.00361
100	8.97	8.99	-0.00130	6.93	6.99	-0.00376

The way the blood absorbs the light in the red and infrared bands are unalike during systole and diastole as can be seen in Fig. 4 (a) and 4 (b), respectively. As for the red band, increasing oxygen saturation will decrease the absorption coefficient of the tissue during systole and diastole whereas reverse relationship can be seen in the infrared band. On different note, the absorption coefficients during diastole are smaller than the absorption coefficients during systole. These values are tally with the physiological assumption as explained in the Background Study section. As a result, the light intensity accumulated at the detector is greatly affected by this absorption trait as highlighted in Table 2. The light intensity during diastole is larger than the light intensity during systole for both wavelengths. Although, the light intensity during diastole is substantially increased as the oxygen saturation increases for the red band, the infrared band shows considerably decreased for the same situation. Using the ratio, R obtained at 660 nm and 890 nm, the ODR for each oxygen saturation level is calculated using Equation 7. Although, for both wavelengths the R-values tabulated in Table 2 are in the negative values, those negative signs will be cancelled out when using the ODR equation. Fig. 8 shows the resulted ODR value against oxygen saturation by means of ASAP simulation. This graph (ODR value against oxygen saturation) is known as calibration curve.

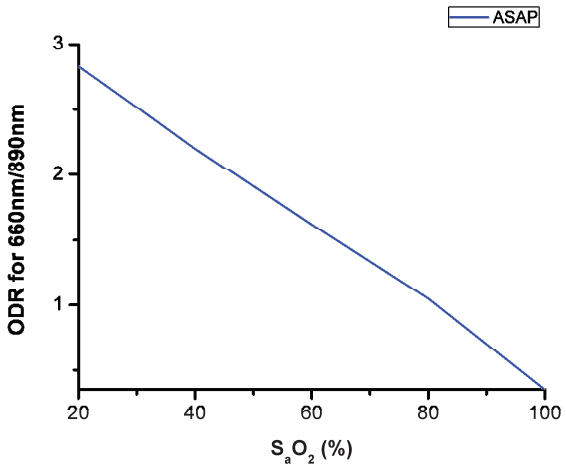

FIGURE 8. Theoretical calibration curve for 660 nm and 890 nm wavelength pair using ASAP software

This main finding obtained in Fig. 8 is then graphically compared with the previous numerical methods namely as Monte Carlo model [2] and Photon Diffusion model [3]. The resulted comparison between ASAP model, Monte Carlo model as well as Photon Diffusion model is visualized in Fig. 9 below. The graphical comparison between the proposed technique and other numerical methods shows an almost identical slope. Therefore, the S_aO_2 error (%) as a function of S_aO_2 is calculated to obtain the statistical differences among these three methods.

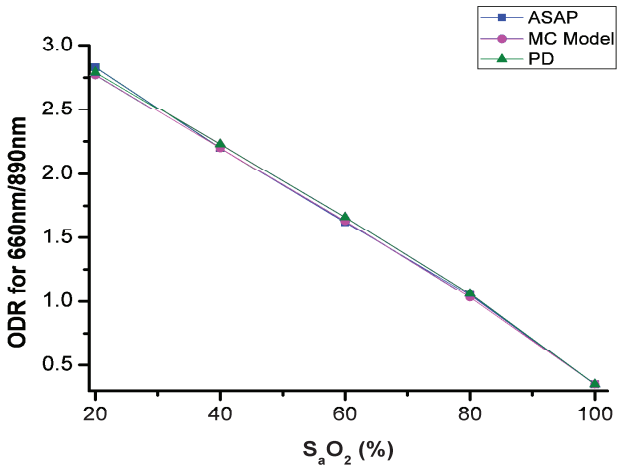

FIGURE 9. Optical density ratio versus oxygen saturation for different methods

TABLE 3. S_aO_2 error (%) between ASAP and the other two methods

S_aO_2 (%)	ASAP versus MC Model (%)	ASAP versus PD (%)	MC Model versus PD (%)
20	**2.17**	1.43	0.72
40	0.00	1.35	1.35
60	0.61	**2.41**	1.81
80	1.94	0.94	**2.83**
100	0.00	0.00	0.00

The data of S_aO_2 error (%) as a function of S_aO_2 can be referred in Table 3 above. The 2.17%, 2.41% and 2.83% are the biggest errors, which occurred between: i. ASAP and Monte Carlo models, ii. ASAP and Photon Diffusion models and iii. Monte Carlo and Photon Diffusion model, respectively. The proposed technique shows zero error at 40 % and 100 % oxygenation as well as at 100 % oxygenation after comparing it with the Monte Carlo model and Photon Diffusion technique, respectively. The reason for comparatively higher differences in the performance of ASAP simulation against Monte Carlo and Photon Diffusion at 20 % and 60 % of oxygen saturation is most probably due to differences in estimation value of calculated absorption coefficient at 20 % and 60 % of saturation. In this research, we had calculated these values by adopting methods as discussed in [4]. Therefore, we speculate that our calculated values maybe slightly different with the absorption coefficient values that were being used previously by the other two numerical methods. It is revealed that the other two methods extracted the values from different sources. Besides that, the Monte Carlo model that is being compared here is based on the Monte Carlo method of [10] whereas the second model utilizes the photon diffusion theory as derived by [3]. The variation of the implemented techniques, though it may not seem to be as the contributed factor, could somehow influence the differences obtained in the statistics results. Nevertheless, the findings from this pilot study shows that the simulation approach using commercial surface-based Monte Carlo software is feasible to produce the theoretical calibration curve. Although, the absorption coefficient of the blood may change due to the physiological factors such as changes in the hematocrit level of blood, the proposed technique can be used to extend the study on the effect of those mentioned factors might have, in assessing the accuracy of pulse oximeter.

CONCLUSION

In summary, relationship between S_aO_2 and optical density during systole and diastole has been mathematically described in this paper. The simulation procedure involving photon tracing from the LED towards the single layer tissue model to obtain the ODR is well elaborated. The proposed method is able to produce the theoretical

calibration curve with minimum error reported. The ASAP simulation gives maximum error at 2.17 %, when compare it with other simulation techniques (Monte Carlo and Photon Diffusion models). Successfully developing the calibration curve via simulation technique is also significant in the pulse oximeter study especially in the area of transabdominal fetal pulse oximeter. Previous researchers for application in transabdominal fetal pulse oximetry have recommended various wavelength pairs and one of the suggested pair is 735nm and 890nm [8-9]. In the future, the methods presented here can be used for modeling the calibration curve for any specific wavelength pairs provided that the corresponding optical properties are correctly defined. Since the relationship of the ODR and S_aO_2 level during SD states has been established, similar experiment can be conducted and tested using other optical simulation environments such as Monte Carlo Multi Layer modeling (MCML) as well as Mesh-Based Monte Carlo method.

ACKNOWLEDGEMENTS

Authors would like to thank BRO for providing Advanced System Analysis Program (ASAP) software (academic license). The authors would like to thank the Ministry of Science, Technology and Innovation as well as Universiti Kebangsaan Malaysia for sponsoring this work under the Research University Grant: 06-01-02-SF0941 and GGPM-2011-074. Also, extended gratitude is expressed to UTHM Contract Research Grant (U565-UTHM) for sponsoring the conference's fee.

REFERENCES

1. A. M. Carter, R. Stiller, V. Konig, J. S. Jorgensen, P. Svendsen and R. Huch, *J Soc Gynecol invest* **5**, 255-259 (1998)
2. P. D. Mannheimer, *Anesth Analg.* **105**, S10-17 (2007).
3. J. M. Schmitt, *IEEE Trans. Biomed. Eng.* **38**, 1194-1203 (1991).
4. P. D. Mannheimer, J. R. Casciani, M. E. Fein and S. L. Nierlich, *IEEE Trans. Biomed. Eng.* **44**, 148-158 (1997).
5. Y. Mendelson, *Wiley Encyclopedia of Biomedical Engineering*, John Wiley & Sons, Inc. New Jeysey (2006).
6. N. A. Jumadi, G. K. Beng, M. A. Mohd-Ali and E. Zahedi, *Optica Applicata* **43**, 747-759 (2013).
7. W. G. Zijlstra, A. Buursma and W. P. Meeuwsen-van der Roest *Clin. Chem*. **37**, 1633-1638 (1991).
8. A. M. Vintzileos, S. Nioka, M. Lake, P. Li, Q. Lou and B. Chance, *Am J Obstet Gynecol*. **192**, 129-133 (2005).
9. A. Zourabian, A. Siegel, B. Chance, N. Ramanujam, M. Rode and D. A. Boas, *Journal of Biomedical Optics* **5**, 391-405 (2000).
10. R. Bonner, R. Nossal, S. Havlin, and G. Weiss, J. Opt. Soc. Amer. A, **4**, 423–432, (1987)